Hearing Research 263 (2010) 216–223

Contents lists available at ScienceDirect

Hearing Research

journal homepage: www.elsevier.com/locate/heares

Research Paper

A method for calibration of bone driver transducers to measure the mastoid impedance

Reggie Weece [a], Jont Allen [b,*]

[a] Department of Mechanical Science and Engineering, University of Illinois at Urbana-Champaign, 1206 W. Green Street, Urbana, IL 61801, USA
[b] Department of Electrical and Computer Engineering, University of Illinois at Urbana-Champaign, 1406 W. Green Street, Urbana, IL 61801, USA

ARTICLE INFO

Article history:
Received 27 August 2009
Received in revised form 19 February 2010
Accepted 23 February 2010
Available online 1 March 2010

ABSTRACT

When using bone vibrator transducers for clinical measurements, the transfer of energy from the bone driver depends on the impedance match between the driver and the load (human mastoid or otherwise) to which the driver will be applied. Current clinical calibration methods are incapable of quantifying this impedance mismatch, hence they fail to account for inter-subject variations of the energy transferred from the driver to the load. This study proposes a straightforward method for determining an absolute field calibration of a Radio Ear B71 bone driver, found by measuring the electrical input impedance of the transducer loaded by known masses. This absolute calibration is based upon a circuit model of the driver, describing it with three frequency-dependent parameters. Once these three parameters are known, measurements of the driver input voltage and current may be used to determine arbitrary mechanical load impedances (such as the *in situ* mastoid impedance), and thus the frequency dependence of the transmitted energy. The results of the proposed calibration method are validated by comparison with direct mechanical measurements using specialized equipment not available in the clinic, and a refined bone driver circuit model is proposed to better capture the observed behaviors.

1. Introduction

Our purpose in calibrating a mechanical transducer is to describe the force $F(\omega)$ and particle velocity $v(\omega)$ produced at the driver's mechanical output, in terms of the voltage $E(\omega)$ and current $I(\omega)$ delivered to its electrical input. The standard clinical approach is to use an artificial mastoid, such as the Brüel and Kjær Artificial Mastoid Type 4930, to measure the bone driver's output force, in response to a known input current (BK4930, 1995). This yields a frequency-dependent transfer function F/I, which is a function of velocity, or equivalently, the mechanical load impedance $Z_L(\omega)$. In general, with the driver mounted on a subject's mastoid, this transfer function may be used to estimate the force $F(\omega)$ applied to the mastoid, based on the electrical stimulus level (ISO 389–3, 1994).

A critical issue with this calibration approach (clinically often overlooked) is that the transfer of energy from the bone driver depends on the impedance match between the driver and the load (artificial mastoid, human mastoid, or otherwise) to which the driver is applied. Specifically, if the impedance (mis)match between the driver and *artificial* mastoid is not the same as that between the driver and *human* mastoid, then the artificial mastoid calibration will not properly predict the force (energy) that is being transferred from the driver to the human mastoid. Therefore when the transfer function from the artificial mastoid calibration is used for measurements of a human mastoid, this implicitly assumes that the artificial mastoid and human mastoid possess identical impedance properties — an assumption that is critically undermined by the fact that the mastoid driving-point impedance is significantly subject-dependent (Håkansson et al., 1986; Flottorp and Solberg, 1976). Measurements utilizing the artificial mastoid calibration suffer from this significant lack of accuracy due to large differences between the impedance of the subject's mastoid and artificial mastoid. Furthermore, because a subject's mastoid impedance can also depend on the placement of the bone driver, repeated measurements of a specific subject may suffer from lack of precision as the bone driver is repositioned between measurements (Flottorp and Solberg, 1976).

In order to quantify and account for these effects, it is necessary to measure the mastoid impedance as seen by the bone driver's diaphragm *each time* it is mounted on a subject's mastoid.[1]

* Corresponding author. Address: 2061 Beckman Institute, 405 N. Mathews, Urbana, IL 61801, USA. Tel.: +1 217 244 9567.
E-mail address: jontalle@illinois.edu (J. Allen).

[1] Much of the discussion in this paper focuses on the specific case of positioning the bone driver on a subject's *mastoid*. However, all statements are applicable to other driver placements, e.g., the forehead. In fact, the problems with typical driver calibration techniques only worsen as the actual load impedances deviate further from the artificial mastoid's impedance.

0378-5955/$ - see front matter © 2010 Elsevier B.V. All rights reserved.
doi:10.1016/j.heares.2010.02.013

The aim of this research is to develop an *absolute* clinical calibration method for the bone driver, the meaning of which is described below in Section 2.1. Such a calibration facilitates the measurement of the mastoid driving-point impedance, as seen by the driver, every time it is used. Knowledge of the *in situ* mastoid driving-point impedance then allows the power transferred to the mastoid to be measured as a function of frequency.

2. Theory

In order to be feasibly implemented in a clinical setting, the calibration method proposed here must rely only on electrical measurements (voltages, currents) or a function of known load impedances. It is of course possible to obtain direct measurements of the mechanical motion of the bone driver diaphragm, but such measurements are complicated and require specialized equipment (such as lasers) not to be found in a clinical setting, due to their cost. For example, Haughton (1982) built a mechanical system for imposing a variable load on a Radio Ear B71 bone vibrator in order to derive its mechanical impedance and transduction coefficient. His analysis assumed that the transducer was reciprocal ($T_{em} = T_{me}$) rather than anti-reciprocal ($T_{em} = -T_{me}$), as required for electromagnetic transducers (Beranek, 1988; Hunt, 1954; McMillan, 1946), thus rendering the results uninterpretable. Cortés (2002) studied the bone driver output force as a function of the input voltage, again relying on expensive mechanical measurements not accessible in the clinic. Cortés did not *assume* reciprocity and found that $T_{em} \approx -T_{me}$, providing experimental confirmation of the driver's anti-reciprocal nature. The present analysis proposes a calibration approach, easily and economically applied in the clinic (i.e., no laser or other special test equipment is required).

2.1. Hunt's transducer model

As depicted in Fig. 1, Hunt (1954) describes an electromechanical transducer as a two-port linear relation: the signals on the electrical side are represented by voltage E and current I, and on the mechanical side by force F and particle velocity v. The electrical and mechanical variables are related by the following two-port equation:

$$\begin{bmatrix} E(\omega) \\ F(\omega) \end{bmatrix} = \begin{bmatrix} Z_e(\omega) & T_{em}(\omega) \\ T_{me}(\omega) & z_m(\omega) \end{bmatrix} \begin{bmatrix} I(\omega) \\ v(\omega) \end{bmatrix}. \tag{1}$$

The transducer has an electrical impedance Z_e, a mechanical impedance z_m, and two transduction coefficients: T_{em} represents the electrical transduction due to mechanical energy, and T_{me} represents the mechanical transduction due to electric energy. Z_e, z_m, T_{em} and T_{me} are each functions of frequency ω. The phase of Z_e and z_m must be limited to $\pm\pi/2$ (Van Valkenburg, 1964). Furthermore, for an anti-reciprocal transducer such as an electromagnetic bone driver (McMillan, 1946), the transduction coefficients are equal but of opposite sign, thus

$$T \equiv T_{me} = -T_{em}. \tag{2}$$

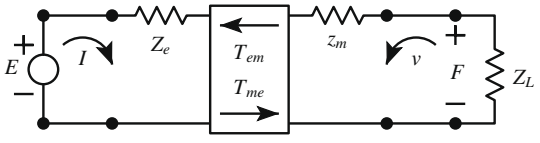

Fig. 1. Schematic representation of an electromechanical transducer, loaded by a mechanical impedance Z_L. The transducer is a two-port model composed of the Hunt parameters Z_e, z_m, T_{me} and T_{em}. Due to reciprocity, $T_{em} = -T_{me}$.

The T_{me} units [N/A] are equivalent to those of T_{em} [V/ms^{-1}]. We shall show later that $T(\omega)$ is "all-pole" and has (at least approximately) the same poles as z_m. Because it is "all-pole", the phase of T is *not* restricted to $\pm\pi$. The only constraint on $T(\omega)$ is that it is causal, and of course, passive.

The three parameters $Z_e(\omega), z_m(\omega)$ and $T(\omega)$ are henceforth referred to as the *Hunt parameters*, and their complex, frequency-dependent values fully characterize the transducer — i.e., we say they form an *absolute* calibration of the driver. It follows that precise knowledge of these three impedance properties facilitates the measurement of arbitrary load impedances and transmitted energy. The purpose of this research then, is to find an effective way to easily and inexpensively estimate the Hunt parameters in the clinical environment (i.e., without requiring direct measurements of the mechanical variables F or v). The proposed method is to accomplish this by analyzing changes in the bone driver electrical input impedance Z_{in} with the driver mechanically loaded by known impedances. Subject to a mechanical load impedance Z_L, based on Eq. (1), the electrical input impedance is

$$Z_{in} \equiv \frac{E}{I} = Z_e + \frac{T^2}{z_m + Z_L}. \tag{3}$$

This calibration method is an extension of the procedure of Allen (1986) for an electroacoustic transducer, which assumed that the effective load of each calibration impedance differed from its physical load, and thus used a least-squares solution to calculate the driver Thevenin properties from an over-determined system of equations.

2.2. Application of the Hunt model

Given estimates $\hat{Z}_e(\omega), \hat{z}_m(\omega)$ and $\hat{T}(\omega)$, any mechanical load impedance Z_L may be determined from the corresponding measured electrical input impedance Z_{in}:

$$Z_L = \frac{\hat{T}^2}{Z_{in} - \hat{Z}_e} - \hat{z}_m. \tag{4}$$

From Eq. (1), the applied mastoid velocity and force are then

$$v = \frac{\hat{Z}_e I - E}{\hat{T}}, \tag{5}$$

and

$$F = -vZ_L = \frac{E - \hat{Z}_e I}{\hat{T}} Z_L. \tag{6}$$

In the clinic, Z_L is the mechanical driving-point impedance of the mastoid bone in series with the dermal cover (skin). Thus the power transferred to the mastoid $\mathscr{P} = Fv$ may be directly estimated from electrical measurements once the Hunt parameters are known.

3. Materials and methods

3.1. Measurement setup

The electrical input impedance to a Radio Ear B71 bone vibrator was measured with the driver loaded by four mass loads, having a mass of 14.541, 35.055, 57.431, and 99.241 g. In electrical terms, masses behave as an inductive load, e.g., $Z_{L|A} = j\omega m_A$, where A $(B, C, \ldots)$ designates one particular mass load condition. The bone driver was oriented face-up so that each mass could be affixed to the diaphragm surface with double-stick tape. The tape layer was thin and light enough to have negligible effect on the measured impedance, while ensuring tight coupling between the movements of the diaphragm and mass; this was necessary to avoid significant nonlinear distortion. Such distortion was also a

concern due to coupling from the driver's backside if placed on a rigid surface. Thus the driver was situated on shallow egg crate foam of 3/8″ thickness. This sufficiently eliminated these artifacts, and further tests, with additional foam, showed no differences in response due to the increased mechanical isolation of the B71.

Voltage signal input/output was performed using an Indigo sound card from Echo Audio. The stimulus waveform was a 24 bit, 2048 point frequency-swept chirp, with a sampling rate of 48 kHz. This yielded a period of 2048/48 ms, corresponding to an FFT frequency resolution of 23.4375 Hz. The signal-to-noise ratio was improved by looping the chirp and averaging at least 500 consecutive buffers, for a total measurement time for each mass of less than 25 s. The 1 V chirp signal was output from the Indigo card to the combined load of the bone driver and a known reference resistor of 99.709 Ω: this choice of voltage and resistance ensured that harmonic distortion of the bone driver was kept at least 50 dB below the fundamental for frequencies between 500 Hz and 8 kHz. The reference resistor was connected between the driver's negative terminal and the sound card ground. From measurements of the output stimulus as well as the voltage response across the reference resistor, the input impedance looking into the driver's electrical terminals was accurately measured (e.g., 10^{-4} relative error) as a function of frequency.

3.2. Laser measurements

In order to verify the Hunt parameter estimations found using the new proposed technique, a laser system was used to directly measure the velocity response of the bone driver loaded by masses of 14.541 and 41.810 g. The bone driver was positioned face-up on a small amount of cotton on a translation stage, which contained mechanisms to provide isolation from tabletop vibrations. The translation stage was used to position the center of the driver diaphragm surface directly below the laser. Preliminary testing (not shown here) revealed that the laser measurements were not adversely affected by nonlinear distortion or slight variations in the positioning of the driver under the laser.

3.3. Bone driver demagnetization

After all other measurements were completed, the bone driver electrical input impedance Z_{in} was measured in an unloaded condition. The driver was then demagnetized and the input impedance $Z_{in|demag} \equiv Z_d$ was measured, again in an unloaded state. In this demagnetized condition, T effectively drops by several orders of magnitude $(T(\omega) \approx 0)$.

3.4. Hunt parameter estimation methods

Although four mass-loaded input impedances were measured, only three were needed to estimate the three Hunt parameters. This three-mass approach — henceforth designated 3M — is the most generic method for performing an absolute calibration of the bone driver, requiring only simple electrical impedance measurements, easily implemented in a clinical setting. However, for research purposes it is helpful to compare with a calibration derived from mechanical measurements. Using the laser measurements of the driver velocity response, only *two* mass-loaded measurements were necessary to determine the transduction coefficient $\tilde{T}$ and mechanical impedance $\tilde{z}_m$; this approach is designated 2ML (2-Mass with Laser). The full details of these Hunt parameter derivations, given the constituent Z_{in} measurements, are presented in Appendix A.

4. Results

4.1. Input impedance of mass measurements

The four mass-loaded driving-point electrical input impedance curves are shown in Fig. 2 as magnitude $|Z_{in}|$ and phase $\angle Z_{in}$. These curves exhibit mechanical resonances that decrease in frequency as the loading mass increases. These resonances consist of a pole (peak in the response) followed at a slightly higher frequency by a zero (valley in the response). The unloaded driver has the highest resonance frequency, with the pole and zero at 1125 and 1195 Hz, respectively. In order from smallest mass to largest mass, the four mass-loaded measurements have pole frequencies of 727, 633, 586 and 563 Hz; the accompanying zero frequencies are 773, 680, 633 and 609 Hz. (Recall that each of these values is limited in accuracy by the 23.4375 Hz FFT frequency resolution.) The second resonance of the four measurements is around 2.75–3 kHz. The DC resistance of the driver coil was estimated as 3.02 Ω.

4.2. Calibration using three mass loads (3M)

Although four different masses were tested, only three are required to calculate the three Hunt parameters using the 3M method. This yields four unique three-mass combinations, each producing a set of estimated Hunt parameters. All four sets of Hunt parameters are plotted in Figs. 3–5.

The estimated electrical impedance $\hat{Z}_e$ in Fig. 3 displays two resonances, with poles at 516 and 2789 Hz and zeros at 563 and 3094 Hz. It is worth noting that the resonances in the electrical input impedance of the mass-loaded driver shift significantly as a function of the load (see Fig. 2), but when these various input impedances are combined as necessary to calculate the estimate

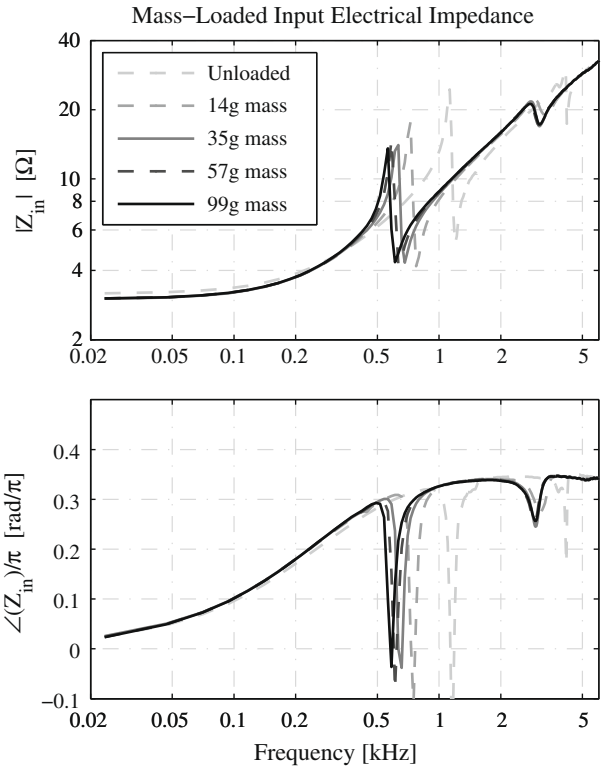

Fig. 2. Magnitude and phase of the bone driver input impedance Z_{in} for the four mass measurements. Each line represents one of the mass loading conditions. The lightest dashed line is for the unloaded driver, and then as the load mass increases, the resonances shift to lower frequencies.

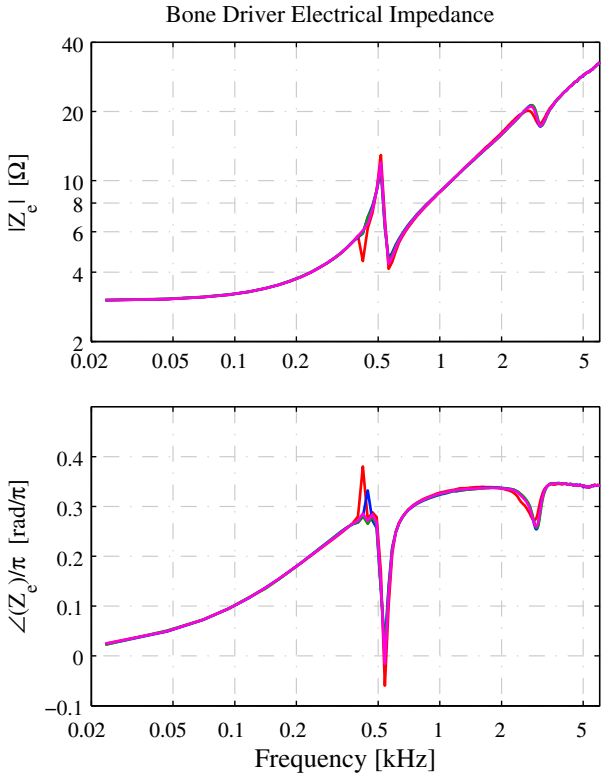

Fig. 3. Magnitude and phase of the Hunt electrical impedance $\hat{Z}_e$, calculated using the 3M method. Each line here represents one of four different combinations of three of the four mass measurements in Fig. 2.

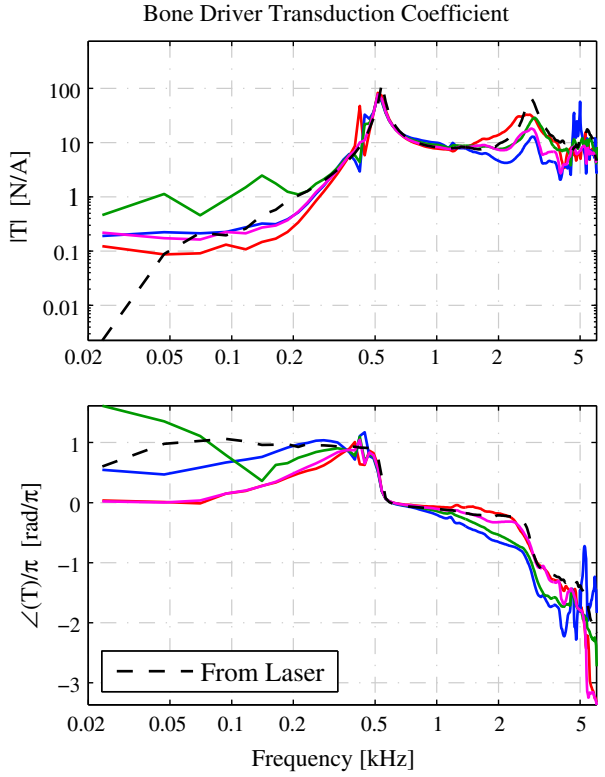

Fig. 4. Magnitude and phase of the Hunt transduction coefficient. Each solid line represents one of four different $\hat{T}$ estimates calculated with the 3M method. The dashed black line is the 2ML result $\tilde{T}$, from laser measurements of the bone driver velocity.

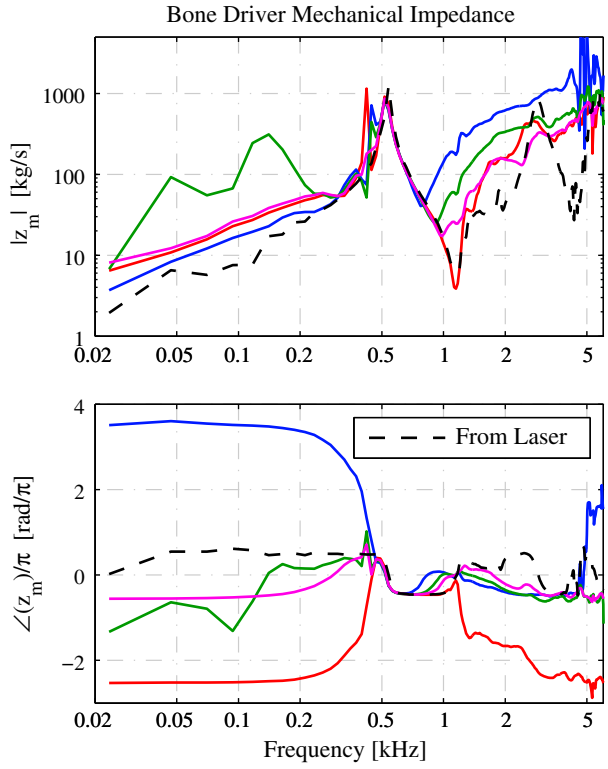

Fig. 5. Magnitude and phase of the Hunt mechanical impedance $\hat{z}_m$. Each solid line represents one of four different $\hat{z}_m$ estimates calculated with the 3M method. The dashed black line is the 2ML result $\tilde{z}_m$, from laser measurements of the bone driver velocity.

of $\hat{Z}_e$, the resulting curves are nearly identical, regardless of which specific input impedances were chosen. The fact that they are not exactly the same reflects measurement errors. At low frequencies, $\hat{Z}_e$ approaches a constant resistance of about 3.02 Ω. The high-frequency behavior is less than a pure inductive rise, as may be seen in the phase, which peaks at 1.09 rad, as opposed to a full $\pi/2 \approx 1.57$ rad, as would be expected for a pure inductor. These results are nearly identical to those found by Cortés (2002), who measured the B71 Hunt parameters using a combination of electrical and mechanical measurements, and found a first resonance in Z_e just above 500 Hz and a second resonance slightly below 3 kHz.

The Hunt parameters in Figs. 3–5 all exhibit disturbances at 422 and 445 Hz. This is due to noise in the root Z_{in} measurements at those two frequency points.

4.3. Calibration using laser measurements (2ML)

Using two mass loads along with the laser system's velocity measurements (denoted 2ML), the transduction coefficient $\tilde{T}$ and mechanical impedance $\tilde{z}_m$ were measured. A tilde is used here to differentiate the laser-measured results from the 3M estimates, which are marked with an over-hat (^). The transduction coefficient $\tilde{T}$ is plotted in Fig. 4 along with the 3M estimate $\hat{T}$. Likewise, the mechanical impedance $\tilde{z}_m$ is shown in Fig. 5 alongside the 3M estimate $\hat{z}_m$.

The estimated transduction coefficients $\hat{T}$ are in general agreement with each other from 300 to 1500 Hz, and match the laser-measured $\tilde{T}$. There are two noticeable peaks, matching the pole frequencies of $\hat{Z}_e$. These results agree both qualitatively and quantitatively with the data of Cortés (2002) and Haughton (1982). For example, they found $\hat{T}$(1 kHz) magnitudes of approximately 8 and 10 N/A, respectively, comparable to values of 8–10 N/A found here.

4.4. Input impedance of demagnetized measurement

Fig. 6 shows the input impedance to the driver before and after demagnetization, which almost completely removes the mechanical resonances. With some manual processing, the very small residual resonances were eliminated from the demagnetized input impedance, as shown in Fig. 7. This smoothed, resonance-free version of the demagnetized input impedance measurement is designated Z_d.

4.5. Model of Z_d from demagnetized measurements

The demagnetized electrical impedance Z_d is validated by comparison with a model proposed by Vanderkooy (1989). This model accounts for the effect of eddy currents in the driver magnet, which reduce the inductive impedance at the expense of loss at high frequencies due to magnetic flux diffusion, leading to a $\sqrt{j\omega}$ behavior. As shown by Warren and LoPresti (2006), the Bessel function ratio in Vanderkooy's model can be expanded as a diffusion ladder network, such that the electrical impedance can be represented by the circuit shown in Fig. 8. This model contains four parameters: the DC resistance R_o, an inductance L_o, the resistance factor R, and shunt inductance factor L. The ladder network parameters R and L are functions of physical properties of the transducer. From Warren and LoPresti (2006) and Vanderkooy (1989),

$$R = \frac{4\pi n^2 l}{\sigma}, \tag{7}$$

$$L = \mu l n^2 \pi r_o^2, \tag{8}$$

where n is the number of coil windings, l is the coil length, σ is the conductivity of the pole structure, μ is the permeability of the pole structure, and r_o is the coil radius.

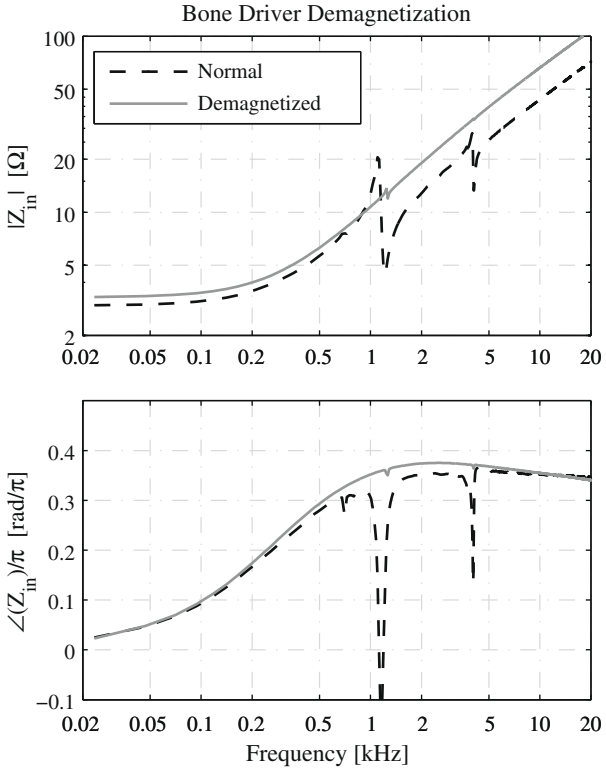

Fig. 6. Magnitude and phase of the input impedance Z_{in} for an unloaded bone driver before and after demagnetization. The residual resonances at 1.25 and 4.06 kHz in the demagnetized data indicate that the demagnetization does not perfectly eliminate all mechanical coupling.

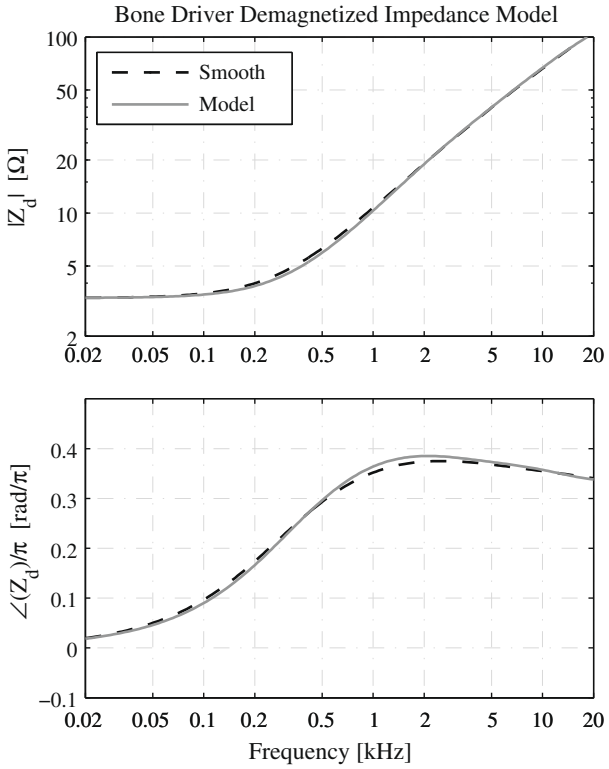

Fig. 7. Magnitude and phase of the demagnetized electrical impedance Z_d, from smoothing the demagnetized measurement in Fig. 6. This dashed line is the result of the model for Z_d (Fig. 8) discussed in Section 4.5.

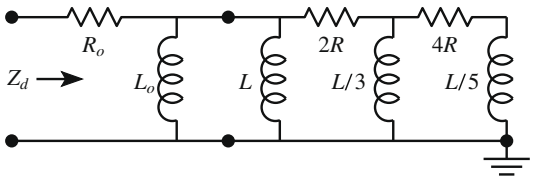

Fig. 8. Circuit diagram of the demagnetized electrical impedance model, defined by the DC resistance R_o, an inductance L_o, and the ladder network resistance factor R and shunt inductance factor L.

Although the ladder network theoretically continues forever, only five terms were needed to give the results shown in Fig. 7. The effect of using more terms is negligible for the frequency range of interest (Warren and LoPresti, 2006). The DC resistance R_o was read directly from Z_d. The remaining three model parameters were found by minimizing the RMS error between the model and Z_d. The final parameter values were $R_o = 3.297\ \Omega, L_o = 2.197$ mH, $R = 44.53\ \Omega$, and $L = 5.024$ mH to yield the curve shown in Fig. 7. The model fits very well, with the exception of some minor phase deviations from 1 to 5 kHz.

5. Discussion

5.1. Comparison of T and z_m with laser measurements

Fig. 4 shows the transduction coefficient $\tilde{T}$ from the laser measurements, along with the $\hat{T}$ estimates from the three-mass measurements. The laser curve exhibits similar behavior to the various derived $\hat{T}$ estimates, and is in excellent agreement with the results of both Haughton (1982) and Cortés (2002). This behavior is an all-pole response, which requires that T represents a delay

line, terminated in an impedance at each end. This interpretation of $T(\omega)$ as an all-pole transfer function seems to have gone unnoticed in previous publications. For example, it is a fundamental departure from Hunt's *assumption* that T is akin to a simple second-order driving-point impedance having the form $T = r_T + j\omega l_T + \frac{1}{j\omega C_T}$ (Hunt, 1954, p. 94). Hunt's model, and thus his proof of physical realizability, must be amended accordingly in order to successfully use it as a basis for calibration.

Looking at Fig. 5, the mechanical impedance behavior is closely related to the transduction coefficient: it contains the same resonances near 0.5, 2.9 and 5.5 kHz, but they are interspersed with antiresonances at 1.2 and 4.3 kHz, as required for a driving-point impedance, having its phase between $\pm\pi/2$. This agrees with the work of other authors (Haughton, 1982; Cortés, 2002). The 3M data is similar, although the four different 3M curves begin to diverge above 800 Hz. Only one of the four curves (the one from the three lightest masses) completely follows the 1.2 kHz antiresonance. The phase data in Fig. 5 reveals a second issue: the phase of a driving-point impedance must remain within $\pm\pi/2$ in order to ensure causality, yet the 3M data clearly does not stay within these bounds due to measurement noise skewing the phase unwrapping. However, even if this phase *unwrapping* issue is temporarily ignored, the phase *values* below 0.3 kHz approach $-\pi/2 \pm 2\pi$. They should instead approach $\pi/2$, indicative of a mass-dominated system.

In order to avoid direct mechanical measurements, the 3M calibration method uses the driver's electrical terminals as a "window" into the Hunt parameters. It is therefore reasonable to suspect that the mechanical impedance data will be of generally lower quality than the electrical impedance and transduction coefficient, because the calibration must "look through" the transduction coefficient to observe the mechanical impedance. From Fig. 4, the transduction coefficient magnitude is small below about 300 Hz, limiting the frequencies at which the electrical input impedance measurements are sensitive to changes in the load (Fig. 2). When these electrical input impedances are then used to calculate the Hunt parameters, the result is a diminished signal-to-noise ratio of the estimated mechanical impedance. The variability seen in the mechanical impedance estimates (Fig. 5) must be resolved before this calibration method can be used to produce accurate mastoid impedance measurements.

5.2. Refined bone driver model

Inspired by the observed resonance/antiresonance structures of z_m and T, an extended transducer model is proposed in Fig. 9. Beginning at the far left, the demagnetized impedance circuit of Fig. 8 is represented with a box labeled "Z_d". Following Cortés (2002), a voltage source and force source are used to signify the transfer of energy between the electrical and mechanical domains. These sources have opposite polarity due to anti-reciprocity, and they are proportional to Bl, where B is the magnetic field strength and l is the length of wire in the voice coil.

The electrical stimulus results in a force source $F_s = Bll$ at the transducer's voice coil, with a resulting source velocity v_s. The physical connections between the voice coil and diaphragm are represented by a spring (series capacitance C) and a mass (shunt inductance m). This then feeds a transmission line with characteristic impedance Z_o, the output of which is the force F and velocity v, where the load impedance Z_L is applied.

For a setup such as this, involving a delay line terminated by various impedances, the relationships between the line's characteristic impedance, its delay τ, and the termination impedances will determine the frequencies of resonance. Furthermore, this type of transmission line setup is in agreement with the all-pole nature of T, and with the z_m behavior described in the previous section.

From Eq. (1), the bone driver mechanical driving-point impedance is defined as the ratio of the output force and velocity when the input current is zero:

$$z_m = \left.\frac{F}{v}\right|_{I=0}. \tag{9}$$

Inspection of Fig. 9 reveals that setting the current to zero effectively open circuits the force source F_s, removing the influence of the capacitor from the circuit. This will cause the circuit to be dominated by the mass at low frequencies, as viewed from the mechanical terminals at the far right. This mass-dominated behavior is evident in Fig. 5, as in the results of Haughton (1982) and Cortés (2002).

5.3. Explanation of Z_e resonances

At first glance, the demagnetized electrical impedance measurement Z_d seems to contradict the $\hat{Z}_e$ results of the three-mass calibration. From Eq. (1), the electrical impedance is given by

$$\hat{Z}_e \equiv \left.\frac{E}{I}\right|_{v=0}. \tag{10}$$

Similarly, demagnetizing the bone driver makes T negligibly small, such that the electrical energy is not transduced into mechanical energy. This makes $v = 0$, so Eq. (3) gives a demagnetized electrical impedance of

$$Z_d = \left.\frac{E}{I}\right|_{v=0}. \tag{11}$$

Based on Hunt's model, it then follows that $\hat{Z}_e$ must equal Z_d, but comparing Figs. 3 and 7 shows that this is clearly not the case.

The refined bone driver model accounts for these observed differences between $\hat{Z}_e$ and Z_d. In Fig. 9, transduction from the electrical domain results in a source velocity $v_s(\omega)$ at the voice coil that is *distinct* from the transducer output velocity $v(\omega)$ at the diaphragm. Hunt's model (and thus Eq. (10)) only concerns the output velocity v, but the logic behind the demagnetized measurement (Eq. (11)) technically applies to v_s, not v. Thus Eq. (11) should be written

$$Z_d = \left.\frac{E}{I}\right|_{v_s=0}. \tag{12}$$

Under this condition of $v_s = 0$, the demagnetized measurement of Z_d will in fact be free from mechanical resonances, as seen in Fig. 7. Likewise, analysis of the circuit model in Fig. 9 reveals that even if the output velocity is zero ($v = 0$), measurements of the

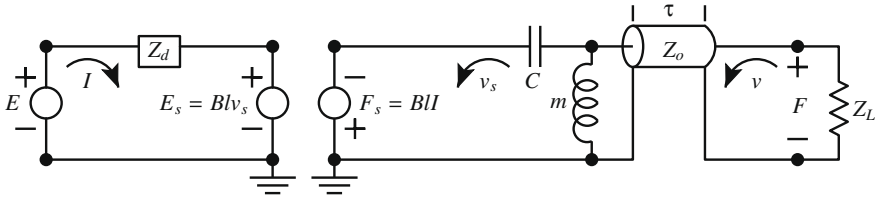

Fig. 9. Refined bone driver model, incorporating a transmission line delay element in the mechanical domain, having delay τ and characteristic impedance Z_o. This delay (τ) would explain the resonant structures at 0.5 kHz in both T and z_m.

electrical input impedance (as defined by Hunt) will still be influenced by the *mechanical* parameters m, C, and Z_o, resulting in the resonances seen in Fig. 3. Although Hunt's approach of modeling the transducer as a two-port network is technically correct, his notation is misleading because the "electrical impedance" Z_e is *not* purely electrical, as it includes mechanical elements C and m, as well as the open-circuited transmission line.

5.4. Summary

Beginning with a two-port transducer model from Hunt (1954), a novel calibration method has been proposed for determining the electrical driving-point impedance $Z_e(\omega)$, mechanical driving-point impedance $z_m(\omega)$, and transduction coefficient $T(\omega)$ for the Radio Ear B71 bone vibrator, based on measurements of the electrical input impedance $Z_{in}(\omega)$ with the driver loaded by three known mass loads. The transduction coefficient estimate $\hat{T}$ from this 3M method has an all-pole response (Fig. 4), in good agreement with the mechanical measurements of Haughton (1982) and Cortés (2002), and the $\widetilde{T}$ found using our direct laser measurements of the transducer output velocity ("2ML"). The mechanical impedance estimate $\hat{z}_m$ should have alternating poles and zeros, as shown by the 2ML measurement $\tilde{z}_m$, but instead deviates from this form above the first resonance frequency (Fig. 5). This reveals a limitation of the 3M method — the driver's mechanical impedance may be estimated from the driver's electrical terminals, only limited by noise or uncertainties in the electrical impedance and transduction coefficient.

The 3M method yields an electrical impedance estimate $\hat{Z}_e$ that contains mechanical resonances (Fig. 3). At first glance, this seems to contradict Hunt's notion of an *electrical* impedance. The demagnetized measurement of Z_d further suggests that the electrical impedance should not contain resonances (Fig. 7). The apparent conflict between the results of Figs. 3 and 7 is due to Hunt's model not making a distinction between the voice coil velocity v_s and the transducer output velocity v. The transducer model proposed in Fig. 9 resolves this apparent discrepancy between $\hat{Z}_e$ and Z_d, and captures the delay line structure of T.

The promising aspect of the 3M absolute calibration approach, as opposed to an artificial mastoid calibration, is that the absolute calibration only requires assumptions about the calibration loads, whereas the artificial mastoid calibration requires assumptions about the (unknown) human mastoid load — namely, that it has the same impedance properties as the artificial mastoid. In order for an absolute calibration method to be clinically viable, it must not rely on flawed assumptions, or measurements that require specialized equipment. Although the $\hat{z}_m$ estimates of the 3M method indicate the need for additional refinement, the $\hat{Z}_e$ and $\hat{T}$ results are in reasonable agreement with the results from complex mechanical measurements (the 2ML laser measurements and the equipment of Haughton and Cortés), yet only require simple electrical input impedance measurements that can be performed in a matter of minutes.

Acknowledgments

The authors are grateful to Daniel Warren and Tom Miller at Knowles Electronics (Itasca, IL) for their gracious help with the demagnetization and laser measurements.

Appendix A. Derivation of the Hunt parameters

A.1. Electrical input impedance

When the bone driver diaphragm is loaded with a mechanical load impedance Z_L, the force and velocity across the load are related by

$$F = -vZ_L. \tag{13}$$

The minus sign is due to the velocity being defined as into the port, as shown in Fig. 1. Inserting Eq. (13) into Eq. (1) and using the reciprocity relation Eq. (2) yields

$$\begin{bmatrix} E \\ -vZ_L \end{bmatrix} = \begin{bmatrix} Z_e & -T \\ T & z_m \end{bmatrix} \begin{bmatrix} I \\ v \end{bmatrix}. \tag{14}$$

From Eq. (14), the bone driver's electrical input impedance Z_{in} is

$$Z_{in} \equiv \frac{E}{I} = Z_e + \frac{T^2}{z_m + Z_L}. \tag{15}$$

An analysis of Eq. (15) reveals that if the transducer were loaded with an infinite load impedance ($Z_L \to \infty$, that is, blocking the diaphragm motion), then the $T^2/(z_m + Z_L)$ term would become negligibly small and the electrical input impedance would equal the transducer electrical impedance ($Z_{in} \to Z_e$). In theory this provides a straightforward method for determining the electrical impedance.[2] In practice it seems impossible to fully block the diaphragm motion — especially in a non-destructive manner — and thus the input impedance will always contain some residual mechanical resonance(s). Instead of using a blocked-motion measurement condition, a system of equations for Z_{in} under three different loading conditions, A–C, is (in theory) equivalent:

$$\begin{aligned} Z_{in|A} &= \hat{Z}_e + \frac{\hat{T}^2}{\hat{z}_m + Z_{L|A}} \\ Z_{in|B} &= \hat{Z}_e + \frac{\hat{T}^2}{\hat{z}_m + Z_{L|B}} \\ Z_{in|C} &= \hat{Z}_e + \frac{\hat{T}^2}{\hat{z}_m + Z_{L|C}}. \end{aligned} \tag{16}$$

Here, the over-hat ($\hat{}$) is used to indicate that $\hat{Z}_e, \hat{T}^2$ and $\hat{z}_m$ are to be estimated from experimental measurements.

A.2. Solving Eq. (16) for the Hunt parameters

The procedure for solving Eq. (16) begins by taking the difference of two of the measurements, eliminating $\hat{Z}_e$ from the equation:

$$Z_{in|C} - Z_{in|A} = \frac{\hat{T}^2}{\hat{z}_m + Z_{L|C}} - \frac{\hat{T}^2}{\hat{z}_m + Z_{L|A}}. \tag{17}$$

Then taking the ratio of two such differences eliminates $\hat{T}$, leaving $\hat{z}_m$ the remaining unknown:

$$\left(\frac{\hat{z}_m + Z_{L|B}}{\hat{z}_m + Z_{L|A}}\right) = \left[\frac{Z_{in|A} - Z_{in|C}}{Z_{in|B} - Z_{in|C}}\right] \left[\frac{Z_{L|C} - Z_{L|B}}{Z_{L|C} - Z_{L|A}}\right]. \tag{18}$$

The term in parentheses on the left side of this equation is a Möbius transformation of the unknown mechanical impedance $\hat{z}_m(\omega)$ (Boas, 1987), and in brackets on the right side are the (known) ratio of input impedance differences and the (known) ratio of load impedance differences. After solving Eq. (18) for $\hat{z}_m$, Eq. (17) may be solved for $\hat{T}^2(\omega)$ and then Eq. (16) for $\hat{Z}_e$.

A.3. Case of known velocity

The laser setup described in Section 3.2 was used to measure the velocity response of the bone driver subject to two different mass loads. From Eq. (14), the two mass loads yield the system of equations

[2] "In theory there is no difference between theory and practice. In practice there is." — Yogi Berra

$$\begin{aligned} -v_A Z_{L|A} &= TI_A + z_m v_A \\ -v_B Z_{L|B} &= TI_B + z_m v_B, \end{aligned} \tag{19}$$

where I_A and v_A represent the current and velocity in the $Z_{L|A}$ loading condition. Simple manipulation of Eq. (19) produces an expression for $\widetilde{T}$ based on the measured velocities, currents, and load impedances:

$$\widetilde{T} = \frac{v_A v_B (Z_{L|A} - Z_{L|B})}{v_A I_B - v_B I_A}. \tag{20}$$

A tilde is used to differentiate $\widetilde{T}$ from the derived estimates $\hat{T}$ or the theoretical value T. Once $\widetilde{T}$ is known, $\tilde{z}_m$ is found using either one of Eq. (19).

References

Allen, J.B., 1986. Measurement of eardrum acoustic impedance. Peripheral Auditory Mechanisms, 44–51.

Beranek, Leo L., 1988. Acoustical measurements. American Institute of Physics.

Boas, R.P., 1987. Invitation to complex analysis. Random House.

BK4930, 1995. Artificial Mastoid — Type 4930. Brüel and Kjær, Skodsborgvej 307, DK-2850 Nærum, Denmark.

Diana Cortés, 2002. Bone conduction transducers: output force dependency on load condition. Technical report. Department of Signals and Systems. Chalmers University of Technology, SE-412 96 Göteborg, Sweden.

Flottorp, Gordon, Solberg, Sigurd, 1976. Mechanical impedance of human headbones (forehead and mastoid portion of the temporal bone) measured under ISO/IEC conditions. The Journal of the Acoustical Society of America 59 (4), 899–906.

Håkansson, Bo, Carlsson, Peder, Tjellström, Anders, 1986. The mechanical point impedance of the human head, with and without skin penetration. The Journal of the Acoustical Society of America 80 (4), 1065–1075.

Haughton, P.M., 1982. A system for generating a variable mechanical impedance and its use in an investigation of the electromechanical properties of the B71 audiometric bone vibrator. British Journal of Audiology 16 (1), 1–7.

Hunt, Frederick V., 1954. Electroacoustics: The Analysis of Transduction and Its Historical Background. Harvard University Press.

ISO 389–3, 1994. Acoustics: reference zero for the calibration of audiometric equipment – Part 3: reference equivalent threshold force levels for pure tones and bone vibrators. International Organization for Standardization, Geneva, Switzerland.

McMillan, Edwin M., 1946. Violation of the reciprocity theorem in linear passive electromechanical systems. The Journal of the Acoustical Society of America 18 (2), 344–347.

Van Valkenburg, M.E., 1964. Network Analysis, 2nd ed. Prentice-Hall, Englewood Cliffs, NJ.

Vanderkooy, J., 1989. A model of loudspeaker driver impedance incorporating eddy currents in the pole structure. J. Audio. Eng. Soc. 37 (3), 119–128.

Warren, Daniel M., LoPresti, Janice L., 2006. A ladder network impedance model for lossy wave phenomena. The Journal of the Acoustical Society of America 119 (5), 3377.